Structural, electronic, and optical properties of medium-sized Li n clusters (n=20, 30, 40, 50) by density functional theory

ARTICLE *in* PHYSICA E LOW-DIMENSIONAL SYSTEMS AND NANOSTRUCTURES · MARCH 2010

Impact Factor: 2 · DOI: 10.1016/j.physe.2010.01.039

5 AUTHORS, INCLUDING:

Bin Lu
University of Tours
5 PUBLICATIONS **8** CITATIONS
SEE PROFILE

Xue Jiang
Dalian University of Technology
25 PUBLICATIONS **189** CITATIONS
SEE PROFILE

Jijun Zhao
Dalian University of Technology
390 PUBLICATIONS **8,432** CITATIONS
SEE PROFILE

Rui-Hua Xie
Xi'an Jiaotong University
154 PUBLICATIONS **1,698** CITATIONS
SEE PROFILE

Physica E 42 (2010) 1755–1762

Contents lists available at ScienceDirect

Physica E

journal homepage: www.elsevier.com/locate/physe

Structural, electronic, and optical properties of medium-sized Li_n clusters (n=20, 30, 40, 50) by density functional theory

Zhao Guo [a], Bin Lu [a], Xue Jiang [a,b], Jijun Zhao [a,b,*], Rui-Hua Xie [c]

[a] School of Physics and Optoelectronic Technology and College of Advanced Science and Technology, Dalian University of Technology, Dalian 116024, China
[b] Key Laboratory of Materials Modification by Laser, Ion and Electron Beams (Dalian University of Technology), Ministry of Education, Dalian 116024, China
[c] Department of Applied Physics, Xi'an Jiaotong University, Xi'an 710049, China

ARTICLE INFO

Article history:
Received 28 December 2009
Received in revised form
24 January 2010
Accepted 25 January 2010
Available online 1 February 2010

Keywords:
Lithium cluster
Electron shell
Polarizability
Optical absorption

ABSTRACT

The lowest-energy structures of medium-sized Li_n (n=20, 30, 40, 50) clusters are determined from simulated annealing technique followed by geometry optimization within the framework of density functional theory. The shapes of magic-number Li_{20} and Li_{40} clusters are nearly spherical while those of the other clusters are ellipsoid. The growth of Li_n clusters is based on core of multi-layered pentagonal bipyramids with other atoms capped on the surface. The binding energies of the Li_n clusters were computed and compared with experiments. At magic-number sizes (n=20, 40), Li_n clusters possess relatively larger HOMO–LUMO gaps and higher ionization potentials, corresponding to the closure of electron shell. The molecular orbitals of the lithium clusters can be grouped into electron shells and their spatial distributions resemble the atomic orbitals. The average polarizability of the Li clusters reduces rapidly with cluster size and can be approximately described by a classical metallic sphere model. The optical absorption spectra of Li_n clusters from time-dependent density functional theory calculations show giant resonance phenomenon, and resonance peak blueshifts with increasing cluster size.

1. Introduction

Lithium is the first metallic element in the Periodic Table of Elements. Lithium atom ($1s^22s$) has a core consisting of two 1s electrons. The 2s valence electron in Li atom cannot penetrate deeply into the core region due to the Pauli Principle [1]. Thus, Li can be considered as an ideal prototype for simple metals. In cluster physics, lithium cluster is a suitable model system for studying many fundamental physical properties of simple metal clusters. It is of interest to explore how the geometric structure, electronic properties, and optical spectrum of a Li cluster evolve as the number of atoms grows from molecular regime to macroscopic scale.

As one of the typical alkali-metal clusters, the mass spectrum of Li clusters exhibits distinct feature of magic numbers associated with electronic shell [2], which can be derived from a structureless jellium model [3]. In the picture of jellium model, the Li atoms are held together by delocalized valence electrons confined in the cluster volume. Hence, these electrons can oscillate collectively and form a plasmon, resulting in the so called "giant resonance" phenomenon in the optical absorption of the medium-sized Li clusters, as it was observed in the Na and K clusters [4,5]. To gain a deeper understanding of the Li clusters beyond the structureless jellium model, first-principles atomistic calculations based on lowest-energy configurations are essential to reveal the correlation between the atomic structures and the electronic/optical properties.

In the past two decades, there have been numerous experimental progresses on the size-selected lithium clusters. Li clusters, which can be generated via supersonic jet expansion or isolated by inert matrix, were investigated via spectroscopic methods including electron spin resonance, infrared, and Raman, etc. [3]. For example, Kornath and co-workers have characterized the small Li_2, Li_4, and Li_8 clusters that were isolated in argon matrices by Raman spectroscopy [6]. Using depletion spectroscopy, optical absorption spectra of small Li_n clusters with n=4–8 were measured and the experimental spectra were interpreted with *ab initio* configuration interaction (CI) calculations [7,8]. Ellert et al. have measured the absolute photoabsorption cross sections for Li_4^+, Li_9^+, and Li_{21}^+ in the optical range and found a significantly smaller oscillator strength than that for sodium [1]. For larger lithium clusters with 100–1500 atoms, Bréchignac and co-workers [8] measured the collective excitation in those clusters and observed a blueshift of the Mie resonance energy with increasing cluster size. Later, the same group [9] studied the dissociation pathways and binding energies of cationic Li_n^+

* Corresponding author at: School of Physics and Optoelectronic Technology and College of Advanced Science and Technology, Dalian University of Technology, Dalian 116024, China.
E-mail address: zhaojj@dlut.edu.cn (J. Zhao).

1386-9477/$ - see front matter © 2010 Elsevier B.V. All rights reserved.
doi:10.1016/j.physe.2010.01.039

clusters up to n=95. The ionization potentials (IPs) of Li_n clusters with up to 26 atom measured by Dugourd et al. [10] showed effects of even–odd oscillations and shell closure at n=8, 20. Using a beam deflection method, Benichou et al. obtained the static dipole polarizabilities of Li_n clusters (n=2–22) and found a coincidence between the static dipole polarizability and the dipole resonance frequency [11]. The same group has also measured the static dipole polarizabilities of small Na–Li mixed clusters with up to eight atoms and performed *ab initio* calculations to compare with experimental data [12].

In current experiments, however, it is hard to determine the geometry structure of an atomic cluster directly. Alternatively, *ab initio* molecular orbital calculations based on the Hartree-Fock (HF) theory and optionally with correlation correction by configuration interaction (CI) method have been performed to explore the ground state configurations and electronic properties of small Li_n clusters. In their pioneering works, Rao et al. [13,14] used unrestricted HF and CI methods to study the small lithium clusters up to five atoms and discussed the size dependence of binding energy and ionization potential. Wang and co-workers [15] carried out HF calculations with the STO-6G and STO-6-21G basis sets on cationic, neutral, and anionic lithium clusters up to seven atoms and compared a number of candidate structures. Using multireference-diexcited configuration interaction (MRD-CI) method, Boustani et al. [16] performed a comprehensive study on the structural and electronic properties of Li_n clusters up to n=14. Sugino and Kamimura [17] developed a variation method based on localized orbital HF theory, which enables them to study the equilibrium geometries and stabilities of Li_n clusters up to n=36. Recently, Wheeler and Schaefer [18] conducted high-level CCSD/cc-pwCVQZ calculations to compute the ionization potentials of small Li_n and Li_nH clusters (n=1–4).

Meanwhile, Kohn–Sham density functional theory (DFT) was also frequently used to investigate lithium clusters with relatively larger size. For small Li_n clusters up to n=20, Gardet and co-workers [19] revealed a structural growth pattern based on pentagonal bipyramid (PBP) and discussed their electronic properties. Within the same size range, Fournier et al. [20] performed a global geometry search for the Li_n clusters using a Tabu search algorithm and found two types of ground state configurations: (i) PBP, icosahedrons and the other related compact structures; (ii) bcc-like structures containing square antiprism. Very recently, Jose and Gadre [21] proposed a molecular electrostatic potential (MESP)-guided method for building Li_n clusters from n=4 to 58 and performed DFT geometry optimization to determine the most stable structures of the small and medium-sized lithium clusters. Using second-order Möller-Plesset (MP2) and B3LYP calculations, Chandrakumar et al. [22] computed a variety of electronic properties of Li_n clusters up to n=10 and found strong correlation between ionization potential and polarizability.

Besides the geometry structures and electronic properties, the optical properties of lithium clusters have been described by different levels of theory. The collective dipole oscillation in a spherical or ellipsoidal distorted metallic droplet can be described by the classical Mie theory [23]. On the other hand, *ab initio* CI calculations were able to reproduce the measured optical spectra of small Li_n clusters up to n=8 [7,8,24,25]. Using time-dependent density-functional theory (TD-DFT), Pacheco and Martins simulated the static polarizabilities and photoabsorption cross section of Li_8 and Li_{20} clusters with equilibrium configurations obtained via Langevin quantum molecular dynamics [26]. In the intermediate size range of n=8–147, jellium model with inclusion of ionic core effects has been employed to compute the Mie resonance in the Li_n and Li_n^+ clusters within the random phase approximation (RPA) [27,28]. In particular, the theoretical optical response of Li_{139}^+ cluster agrees well with the measured data [27].

Except for few studies [17,21], previous theoretical calculations on Li_n clusters were mainly restricted in the small sizes with $n \leq 20$. Much less is known about the medium-sized lithium clusters, which constitute a bridge between the molecular regime and the macroscopic scale. In this paper, we performed an unbiased search for the lowest-energy structures of medium-sized Li_n clusters (n=20, 30, 40, 50) using molecular dynamics simulated annealing method and density functional theory. Comparison between the magic-number clusters (Li_{20} and Li_{40}) with the other sized ones (Li_{30} and Li_{50}) shows distinct effects of delocalized valence electrons and electron shell on the geometry structures, electronic states, HOMO–LUMO gaps, ionization potentials, static dipole polarizabilities, and optical absorption spectra. Giant resonance in the photoabsorption spectra owing to plasmon excitation was also observed.

2. Theoretical methods

In cluster physics, determining the ground state structure of a medium-sized cluster is a challenging task due to the existence of numerous structural isomers on the potential energy surface (PES). In this work, we carried out an unbiased search of the global minimum structures of Li_n (n=20, 30, 40, 50) clusters via simulated annealing (SA) technique incorporated with first-principles molecular dynamics (FPMD). The FPMD simulations were performed using spin-restricted all-electron density functional theory and the double numerical plus p and d polarization (DNP) basis set [29], as implemented in the $DMol^3$ code [30]. The local density approximation (LDA) was adopted to describe the exchange-correlation interaction, which was found to be able to describe the relative energies of different structures of lithium clusters [19]. The Harris functional approximation [31] was used to compute the total energies and forces in a non-self-consistent-field (non-SCF) way.

During the simulated annealing of Li_n (n=20, 30, 40, 50) clusters, the initial configurations were generated randomly. For each size, the cluster structure was annealed independently from a high temperature of 1000 K (about the melting point of lithium solids) down to 300 K by FPMD. The temperature was reduced systematically by 50 K increments. At each temperature, MD simulation in NVT ensemble lasts for 50 ps with a time step of 1 fs (i.e. 50 000 MD steps). Hence, the total simulation time reaches 0.7 ns or 700 000 MD steps for each cluster. To ensure that the simulation time is long enough, for Li_{20} we have performed several independent FPMD-SA simulations and arrived at the same final structure.

The final structures of Li_n clusters from first-principles simulated annealing were further optimized using the same $DMol^3$ code with a more accurate triple numerical basis set including d and p polarization functions (TNP). In the final geometry optimizations, the exchange-correlation interaction was treated by the generalized gradient approximation (GGA) with the Perdew-Burke-Enzerhof (PBE) parameterization [31], which shows best overall agreement with the cohesive energies and Murnaghan equation-of-state parameters of alkali metals (including Li, Na, K) [32]. The equilibrium lattice constants of Li solid from our PBE/TNP calculations is 3.450 Å, in reasonable agreement with experimental value of 3.477 Å [33]. Self-consistent field calculations were done with a convergence criterion of 10^{-6} Hartree on the total energy. All cluster structures were fully optimized without any symmetry constraint with a convergence criterion of 0.002 Hartree/Å for the forces and 0.005 Å for the displacement. The accuracy of the present PBE/TNP method has been assessed by benchmark calculations on the small Li_2 and Li_4 clusters, which will be described in the Section 3.1.

The optical properties including the static dipole polarizability and optical absorption spectrum of Li_n (n=20, 30, 40, 50) clusters in their lowest-energy structures were also investigated by DFT calculations with B3LYP functional [34], as implemented in the GAUSSIAN 03 program [35]. Compared to the PBE functional used in the structural relaxation, the B3LYP functional describes the optical properties of Li clusters more accurately. For example, the TD-DFT/B3LYP/3-21+G calculations of a rhombus Li_4 cluster predicted five main absorption peaks at 1.72, 2.13, 2.31, 2.68, and 3.01 eV, respectively, which agree well with experimental values (1.80, 2.08, 2.36, 2.65, and 2.93 eV) [24]. In contrast, the PBE calculations only yielded four main peaks (1.55, 2.15, 2.72, and 3.02 eV). Static polarizability have been computed with the 6-31+G(d, p) basis set. Meanwhile, TD-DFT method [36,37] was utilized to compute the optical properties (excitation energies, oscillator strengths, and resonance energies) of these lithium clusters. To describe the optical response due to plasmon excitation, we computed 200, 480, 600, and 1200 singlet-to-singlet excited energies for Li_{20}, Li_{30}, Li_{40}, and Li_{50} clusters, respectively. Test calculations show that the numbers of the excitation states considered here guarantee good convergence in the optical absorption spectra and more excitations would not change the resonance frequencies and shape of the spectra. Due to the tremendous demands of compute time, we adopted the 3-21+G basis set in the TD-DFT calculations. Again, test calculations on the optical properties of Li_2 and Li_4 show the validity of the present TD-DFT/B3LYP/3-21+G scheme, and the details will be given in Section 3.1.

3. Results and discussion

3.1. Benchmark calculations on small-sized Li_2 and Li_4

In Table 1, we compared the geometry parameters, binding energies, vibrational frequencies, ionization potentials, and resonance peak frequencies for optical absorption spectra of Li_2 and Li_4 clusters from our theoretical calculations with the available experimental data [9,10,24,38]. For the Li_2 dimer, the theoretical bond length of 2.68 Å is close to the experimental length of 2.67 Å [38], whereas the present PBE/TNP calculations underestimate the binding energy by about 0.07 eV/atom. The vibrational frequency for Li_2 in its equilibrium configuration is 407 cm^{-1}, somewhat higher than the experimental value of 351 cm^{-1} [38]. The vertical ionization potential of Li_2 (5.09 eV from PBE/TNP calculations) also agree well with the experimental IP of 5.14 eV [10]. The resonance peaks in the optical absorption spectrum of Li_2 from our TD-DFT calculations locate at 2.56 and 1.97 eV that are comparable to the experimental values of 2.58 and 1.80 eV [24].

For the Li_4 cluster with planar rhombus configuration, our theoretical calculations at PBE/TNP level overestimate the binding energy by about 0.08 eV/atom. The theoretical vertical IP of Li_4 is 4.4 eV, in agreement with the experimental value of 4.31 eV [10]. The vibrational frequencies for the Raman-active modes of Li_4 are 231, 302, and 380 cm^{-1} from our PBE/TNP calculations, systematically higher than the experimental values of 200, 235, and 327 cm^{-1} [6]. Hence the current PBE/TNP method may overestimate the strength of interatomic bonding to a certain extend, as we will find in the following Section 3.2. The photoabsorption profile of Li_4 exhibit multiple peaks, which locate at 1.72, 2.13, 2.31, 2.68, 3.01 eV from our theoretical calculations and agree well with experimental values at 1.80, 2.08, 2.36, 2.65, 2.93 eV [24], respectively.

Overall speaking, the present theoretical approaches are able to reproduce the structural, electronic, vibrational, and optical properties of small lithium clusters in a rather satisfactory manner. Thus, they can be further applied to describe the larger Li_n clusters with $n \geq 20$, for which some of the physical properties are not available in experiments.

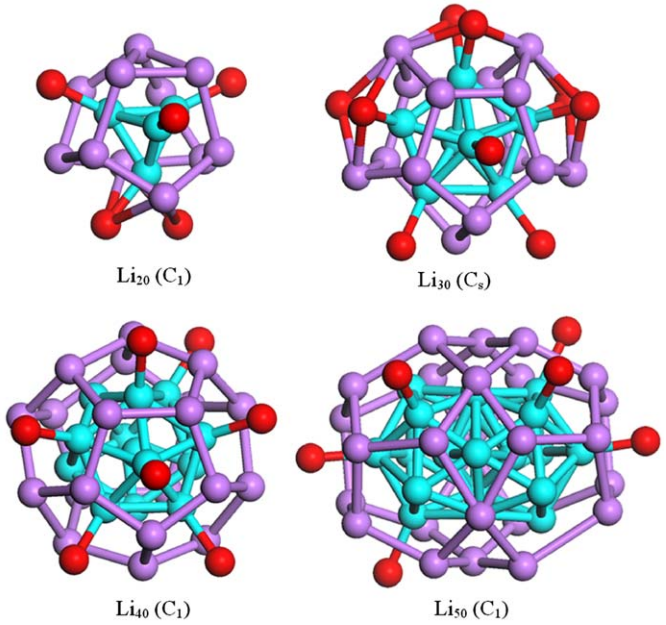

Fig. 1. (Color online) Lowest-energy structures of Li_n clusters (n=20, 30, 40, 50). The point group symmetry for each cluster is given in parentheses. Different colors present different layers of the Li clusters, i.e., turquoise for the core, purple for the frame cage, red for the atop atoms.

Table 1
Li–Li distance (r_0), binding energy (E_b), ionization potential (IP), vibrational frequencies (ω_{vib}), and optical resonance peaks (ω) for Li_2 and Li_4 clusters from our theoretical calculations and experiments.

Li_2	r_0 (Å)	IP (eV/atom)	E_b (eV/atom)			ω_{vib} (cm^{-1})		ω (eV)		
PBE/TNP	2.68	5.09	0.46			407		2.56		1.97
Expt.[a]	2.67	5.14	0.53			351		2.58		1.80
Li_4	IP (eV/atom)	E_b(eV/atom)	ω_{vib} (cm^{-1})			ω (eV)				
PBE/TNP	4.40	0.71	231	302	380	1.72	2.13	2.31	2.68	3.01
Expt.[b]	4.31	0.63	200	235	327	1.80	2.08	2.36	2.65	2.93

[a] Reference [9,10,24,38].
[b] Reference [6,9,10,24].

3.2. Structures and binding energies of medium-sized Li_n (n=20, 30, 40, 50)

The lowest-energy configurations for Li_n clusters (n=20, 30, 40, 50) determined from the combination of FPMD-simulated annealing and PBE/TNP geometry optimization are displayed in Fig. 1. Similar to previous theoretical findings [19–21], our unbiased search reveals a structural growth mechanism based on multi-layered pentagonal bipyramids. In each cluster, certain number of pentagonal bipyramids are stacked together alternatively by sharing the atop atoms, forming a pentagonal cylinder with spiral surface and one atomic strand in the center. Careful examinations show that the core of Li_{20}, Li_{30}, Li_{40}, and Li_{50} are tetrahedron, pentagonal bipyramids, icosahedron and double icosahedron, respectively. The other Li atoms surround the core nearly uniformly. However, these atoms actually distribute at different heights. Except that Li_{30} has C_s point group symmetry, the other sized clusters, i.e., Li_{20}, Li_{40}, and Li_{50}, only have C_1 symmetry.

Moreover, as shown in Fig. 1, the structures of the magic-number clusters, namely, Li_{20} and Li_{40}, are nearly spherical, whereas the shapes of other clusters (Li_{30} and Li_{50}) significantly deviate from a sphere. The overall shape of a cluster can be quantitatively described by the normalized moments of inertia [39] defined as

$$\langle I_i \rangle = 3I_i / \sum_{j=1,3} I_j, \quad (1)$$

where I_i are the principal moments of inertia at the three axis directions (i=x, y, z). According to the above definition, the normalized moments in all three directions should equal to one for a spherical cluster. For a prolate structure, two normalized moments are larger than one while the third moment is less than one; for a oblate structure, two normalized moments are less than one while the third moment is larger than one [39]. The normalized moments of Li_n clusters (n=20, 30, 40, 50) are presented in Fig. 2, which shows spherical shape in the magic-number Li_{20} and Li_{40} clusters as well as the non-spherical shape in the Li_{30} and Li_{50} clusters. The coincidence between the cluster shape and the magic numbers due to closure of electronic shell suggests the validity of shell model in the medium-sized Li_n clusters, as we will further demonstrate in the following discussions.

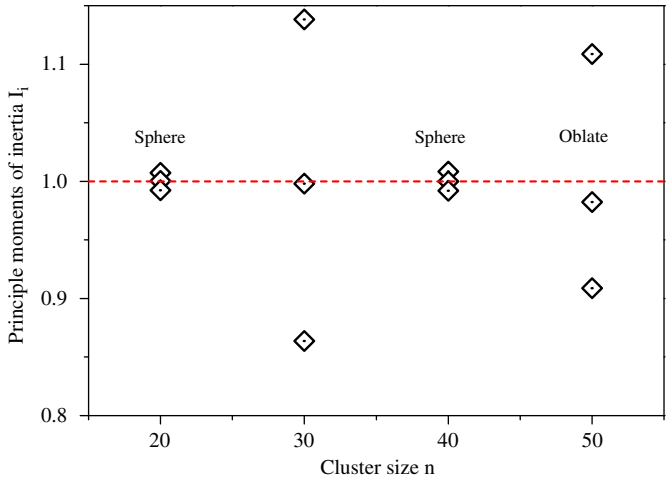

Fig. 2. Normalized moments of inertia at three axis directions for Li_n clusters of different sizes (see Eq. (1) for definition).

Previously, the lowest-energy structure of Li_{20} clusters has been explored by DFT calculations by Gardet [19] and Jose [21]. Both of them considered two candidate configurations based on the double icosahedron. As shown in Fig. 3, the C_{2v} structure can be constructed via adding one atom on the waist of a double icosahedron, and the C_s one can be obtained by capping two atoms on the upper side of an incomplete double icosahedron (with one atom lacking on the bottom). Upon optimization at the same PBE/TNP level, the present lowest-energy configuration of Li_{20} from FPMD-simulated annealing is energetically more favorable than the C_{2v} and C_s isomers by 0.62 and 0.59 eV, respectively. In previous studies of coinage metal clusters [40,41], it was found that Au_{20} (and perhaps Ag_{20}) adopts a highly symmetric tetrahedral structure (T_d). We have considered such tetrahedral configuration for Li_{20} but it is 1.76 eV less preferred in energy with respect to our lowest-energy structure. It is also noteworthy that the energy differences between the three isomer structures in Fig. 3 and the present lowest-energy configurations from the LDA/DNP calculations with Harris approximation are: 0.96 eV (C_s), 1.25 eV (C_{2v}), and 4.21 eV (T_d), respectively. Compared with the more accurate PBE/TNP results, the approximate Harris-LDA/DNP method used in the FPMD simulation is able to reproduce the energy sequence of these isomers but systematically overestimates the absolute values of the energy differences.

Due to the extreme complexity of the cluster PES, it is insufficient to construct the most stable structure of a medium-sized metal cluster simply by following some presumed structural

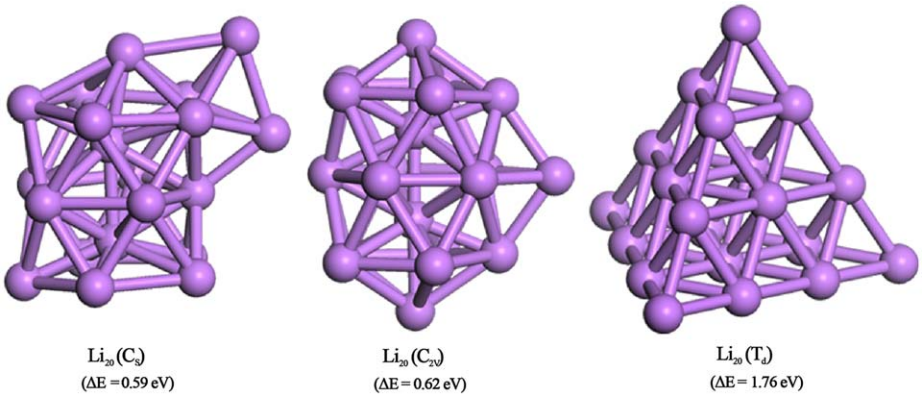

Fig. 3. (Color online) Metastable isomer structures of Li_{20} reported previously in literature [19,21]. The point group symmetry and the energy difference with regard to the lowest-energy configuration for each isomer are given in parentheses.

Table 2
Binding energy (E_b), HOMO–LUMO gap, and vertical ionization potential (VIP) for Li_{20}, Li_{30}, Li_{40}, Li_{50} clusters from the present PBE/TNP calculations.

Clusters	Li_{20}	Li_{30}	Li_{40}	Li_{50}
E_b (eV/atom)	1.25 (1.04)	1.31 (1.10)	1.39 (1.14)	1.41 (1.17)
HOMO-LUMO gap (eV)	1.01	0.28	0.54	0.31
VIP (eV)	4.01	3.66	3.69	3.58

The experimental binding energies estimated using Eq. (2) in Ref. [9] are given in parentheses.

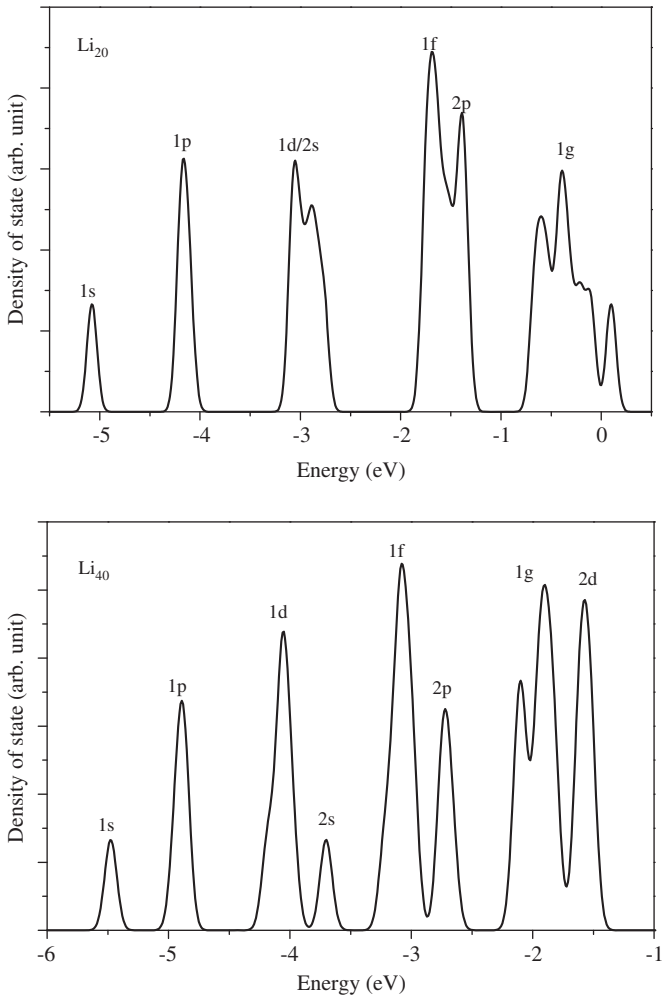

Fig. 4. Electron density of states of the magic-number Li_{20} and Li_{40} clusters (with Gaussian broadening of 0.05 eV). The electron shells (1s, 1p, 1d, …) are labeled.

patterns with relatively high symmetry. Instead, an unbiased search using simulated annealing or other global minimization methods is crucial to reveal the most stable structure and to understand the growth mechanism of these medium-sized clusters. Even though we cannot guarantee that the present lowest-energy structures are the true global minima, the general trend for the size-dependent growth behavior would be still valid.

In Table 2, we listed the theoretical binding energies of Li_n clusters (n=20, 30, 40, 50), along with the experimental data calculated from the Eq. (34) in Ref. [9]

$$E_b(n) = a_v - a_s n^{-1/3}, \quad (2)$$

where a_v=1.52 eV and a_s=1.292 eV are the coefficients fitted to the experimental binding energies [9]. In general, the binding energy of lithium cluster increases as the cluster size increases. Our theoretical calculations are able to reproduce such trend reasonably well. However, the present theoretical method systematically overestimates the binding energy by about 0.2–0.25 eV/atom. Accordingly, the cohesive energy per atom computed for the bcc solid of lithium is 1.81 eV at the same PBE/TNP level of theory, which is 0.18 eV higher than the experimental value of 1.63 eV [42]. From our calculations, the binding energy of the largest Li_{50} cluster is 1.41 eV, approaching 78% of the theoretical cohesive energy of bulk Li solid.

3.3. *Electronic structures of medium-sized Li_n (n=20, 30, 40, 50)*

Since lithium is an alkali-metal element with delocalized 2s valence electron, the electronic structures of Li_n clusters are expected to be described by the jellium model. According to the structureless jellium model [3,43], Li_{20} and Li_{40} with totally twenty and forty valence electrons are the magic-number clusters with closed electron shells (e.g., 1s, 1p, 1d, 2s, …). Fig. 4 plots the electronic density of states (DOS) of Li_{20} and Li_{40} clusters. Interestingly, the energy levels (or molecular orbitals) of valence electrons can be identified into groups that correspond to the discrete 1s, 1p, 1d, 2s, 1f, 2p, 1g, and 2d shells predicted by the jellium model [3]. Twenty electrons (in Li_{20}) is sufficient for filling molecular orbitals up to the 2s shell, while forty electrons (in Li_{40}) corresponds to the closure of the 2p shell.

In Fig. 5, we examine the spatial distribution of the delocalized electrons by plotting the isosurfaces of several representative molecular orbitals of Li_{20}, corresponding to one of the 1s, 1p, and 1d levels in Fig. 4. The shapes of these molecular orbitals resemble the conventional atomic orbitals, that is, a sphere for the s orbital, a dumbbell for the p orbital, and four pear-shaped balls for the d orbital, respectively. This indicates that the medium-sized Li clusters with certain amount of delocalized electrons can be considered as superatom with atomic-like molecular orbitals with shell structure.

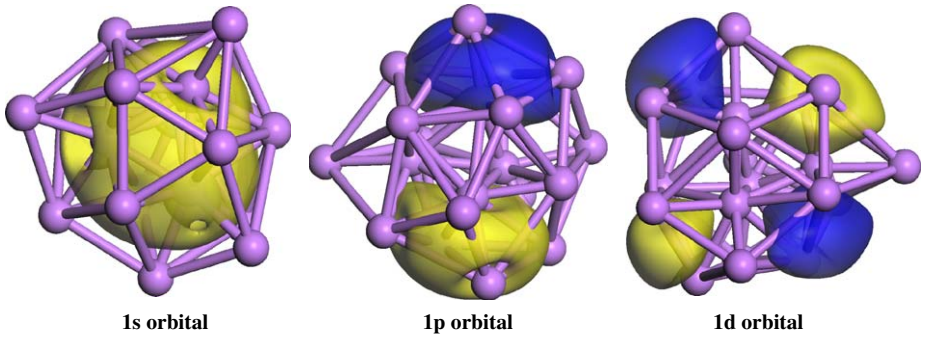

Fig. 5. (Color online) Isosurfaces for the occupied 1s, 1p, and 1d molecular orbitals of Li_{20} cluster. Yellow and blue colors denote the wavefunction phases.

Table 3
Polarizability along three principal axes (α_{xx}, α_{yy}, α_{zz}) and average polarizability $\langle\alpha\rangle$ compared with experimental values [11] in parentheses; optical resonance peaks (ω_1, ω_2) for Li_n clusters (n=20, 30, 40, 50) and the Mie frequency estimated from Eq. (3).

Clusters	Li_2	Li_8	Li_{20}	Li_{30}	Li_{40}	Li_{50}
α_{xx} (Å^3 per atom)	12.20	11.16	8.50	9.44	7.92	9.12
α_{yy} (Å^3 per atom)	12.20	11.14	8.45	9.14	7.87	7.18
α_{zz} (Å^3 per atom)	19.79	11.10	8.58	6.56	7.84	6.66
$\langle\alpha\rangle$ (Å^3 per atom)	14.71 (16.40)	11.14 (10.40)	8.53 (8.90)	8.38	7.88	7.65
ω_1 (eV)	2.56	2.76	2.81	3.34	2.93	3.20
ω_2 (eV)	1.97	2.26		2.79		2.83
Mie frequency (eV)	2.03	2.33	2.66	2.69	2.77	2.81

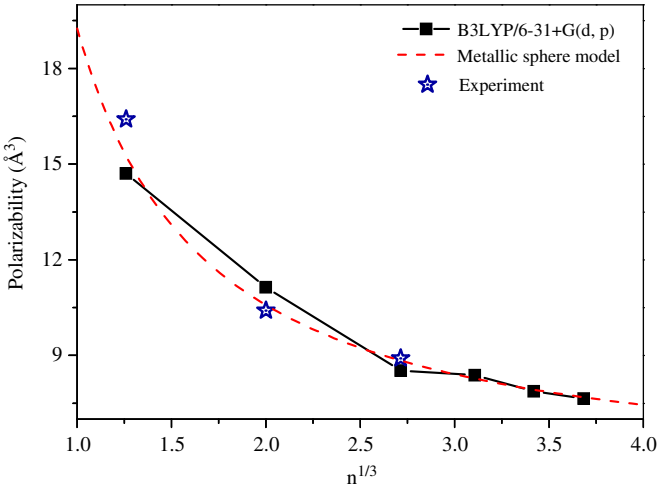

Fig. 6. Average static polarizability per atom of Li_n clusters (n=2, 8, 20, 30, 40, 50) from B3LYP/6-31+G(d, p) calculations (filled squares connected by solid line), empirical curve by classical model of metallic nanometric sphere (Eq. (2)) using the parameters r_s=1.71 Å and δ=0.97 Å (dashed line), and experiment (stars) [11].

The closed electron shell in these magic-number clusters can be further seen in the theoretical gaps between the highest occupied molecular orbital (HOMO) and the lowest unoccupied molecular orbital (LUMO). As shown in Table 2, the HOMO–LUMO gaps of Li_{20} and Li_{40} are 1.01 and 0.54 eV, respectively, significantly higher than the gap values for Li_{30} (0.28 eV) and Li_{50} (0.31 eV).

In Table 2, we also present the vertical ionization potential (VIP) calculated from the differences of total energies between the neutral and cationic clusters within the same equilibrium configuration of the neutral cluster. In general, the values of VIPs decreased as cluster sizes increases. However, the magic-number clusters with closed electron shell possess higher ionization potentials. For example, the computed VIP of Li_{40} is 3.69 eV, higher than that of Li_{30} (3.66 eV). For Li_{20}, our theoretical calculations predicted a vertical IP of 4.01 eV and an adiabatic IP of 3.91 eV; the latter value is higher than the (adiabatic) IP of 3.31 eV from Dugourd's experimental [10]. Similar overestimation of ionization potentials was found in previous theoretical calculations of small Li_n clusters with n=5–20 [20].

3.4. Optical properties of medium-sized Li_n (n=20, 30, 40, 50)

Based on the lowest-energy configurations obtained for Li_n clusters (n=20, 30, 40, 50), the polarizabilities α_{ii} along three principal axes (i represents x, y, z) and the average polarizability $\langle\alpha\rangle$ of these clusters were calculated using the B3LYP/6-31+G(d, p) method. To understand the size-dependent behavior better, we also computed the polarizability and optical response of a small Li_8 cluster with tetra-capped tetrahedral configuration (T_d) [16,24]. The theoretical results are summarized in Table 3, along with the experimental polarizabilities of Li_2, Li_8, and Li_{20} clusters [11]. Within the small size range of n=2–20, the average polarizability decreases rapidly with increasing cluster size and our theoretical results are close to the experimental values with deviation by about 5–10%. As cluster size further increases, our B3LYP/6-31+G(d, p) calculations show that the average polarizability only reduces slowly with the number of atoms.

As shown in Fig. 6, the general trend of average polarizability $\langle\alpha\rangle$ as function of cluster size (or the number of atoms, n) can be fitted to a classical model of metallic nanometric sphere [11,24], i.e.,

$$\langle\alpha\rangle = (n^{1/3}r_s + \delta)^3, \tag{3}$$

where r_s is the Wigner–Seitz radius and δ is an electron spillout parameter. In Ref. [11], these parameters were chosen as r_s=1.75 Å and δ=0.75 Å, whereas fitting our theoretical data in Table 3 yields r_s=1.71 Å and δ=0.97 Å. Again, the applicability of such classical metallic sphere model implies that the lithium cluster starts to behave like a piece of bulk solid even at relatively small size.

In addition to the average polarizabilities, Table 3 also listed three polarizability components α_{ii} along the principal axis directions for each cluster. The effect of cluster shape is clearly reflected by these polarizabilities. For the three magic-number clusters (Li_8, Li_{20}, and Li_{40}) with nearly spherical shape, the three polarizability components are nearly identical, whereas the polarizabilities along the three principal axes are anisotropic for those non-spherical clusters like Li_2, Li_{30}, Li_{50}. A previous DFT calculation of Li_8 [12] predicted the three polarizability components as 11.2, 11.2, and 10.9 Å^3 per atom, respectively, rather close to the present results of 11.16, 11.14, and 11.10 Å^3 per atom. For Li_{20}, previous theoretical values of average static polarizability are 8.56 [11] and 8.04 Å^3 per atom [26], respectively, both are comparable to our theoretical value of 8.53 Å^3 per atom.

We further simulated the optical absorption spectra of the medium-sized Li_n clusters using the TD-DFT/B3LYP/3-21+G method. The theoretical spectra are displayed in Fig. 7, from which one can see the behavior of giant resonance owing to plasmon oscillation. The resonance absorption peaks are labeled in Fig. 7 and summarized in Table 3. For those magic-number clusters at n=20, 40, there is only one major resonance absorption peak, while the non-magic-number clusters exhibit double resonance peaks. Generally speaking, the position of the resonance peak blueshifts with increasing cluster size, in agreement with experimental observation [1,4,8]. For example, the resonance peak energy is

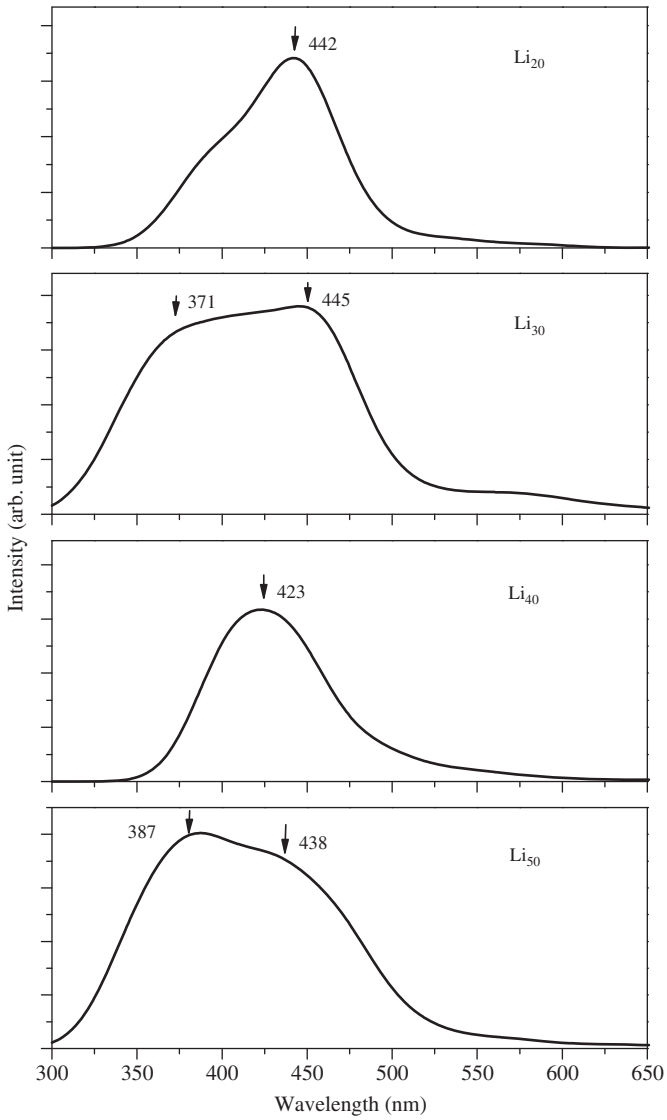

Fig. 7. Optical absorption spectra of Li_n clusters (n=20, 30, 40, 50) (with a Gaussian broadening of 20 nm). The peak values of the resonance absorption peaks are labeled.

2.81 eV for Li_{20}, while it is 2.93 eV for Li_{40}. Moreover, the simulated absorption spectrum for the neutral Li_{20} cluster resembles the measured one for the cationic Li_{21}^+ [1]; both exhibiting one single resonance peak (with peak value at 2.81 eV from the present TD-DFT calculations and at ~2.95 eV from experiment).

For a metallic sphere, the Mie frequency ω_M of optical resonance can be directly related to it polarizability [11],

$$\omega_M{}^2 = \frac{e^2 N^{eff}}{m^* \alpha}. \quad (4)$$

Here N^{eff}=0.77n is the effective number of active electrons in the Li_n cluster and m^*=1.4m_e is the effective electron mass [27]; α is the average polarizability from the above theoretical calculations. As shown in Table 3, the Mie frequencies estimated from the Eq. (4) can roughly reproduce the resonance absorption energies from our TD-DFT calculations. For the magic-number clusters of Li_{20} and Li_{40}, the Mie frequencies are lower than the resonance peak values by about 0.15 eV. For the non-magic-number clusters (Li_{30} and Li_{50}), the Mie frequencies are closer to the resonance energies of the lower-energy peaks.

4. Conclusions

To summarize, we have performed unbiased search for the lowest-energy structures of Li_n clusters (n=20, 30, 40, 50) using first-principles DFT approaches combined with molecular dynamics simulated annealing. A structural growth pattern based on multiple pentagonal bipyramids was revealed and the most stable structure found for Li_{20} is more favorable over the previous proposed ones. The normalized moments of inertia show that the magic-number clusters (n=20, 40) are nearly spherical while other sized clusters are ellipsoid. A variety of cluster properties, including the binding energy, ionization potential, polarizability, and optical absorption, were computed and compared reasonably well with available experimental data. The molecular orbitals of the magic-number Li_n clusters group into electron shells and distribute in space like the conventional atomic orbitals. At the magic-number sizes, Li_n clusters possess relatively larger HOMO–LUMO gaps, higher ionization potentials, and single resonance peak, in agreement with electron shell model. Moreover, the significant reduction of polarizability with cluster size and the onset of giant resonance peaks in the medium-sized clusters validate the picture of jellium model, in which the delocalized valence electrons are restricted in the (spherical) cluster volume. The present atomistic simulation with first-principles methods provide a systematical theoretical description of the medium-sized Li_n clusters, which is helpful for gaining deeper insights in the simple metal clusters.

Acknowledgements

This work was supported by Undergraduate Innovative Research Training Program (081014115) and the Program for New Century Excellent Talents in University of China (NCET-060281) provided by the Ministry of Education of China.

References

[1] C. Ellert, M. Schmidt, C. Schmitt, H. Haberland, C. Guet, Phys. Rev. B 59 (1999) R7841.
[2] W.D. Knight, K. Clemenger, W.A. de Heer, W.A. Saunders, M.Y. Chou, M.L. Cohen, Phys. Rev. Lett. 52 (1984) 2141.
[3] W.A. de Heer, Rev. Mod. Phys. 65 (1993) 611.
[4] C. Bréchignac, J.P. Connerade, J. Phys. B 27 (1994) 3795.
[5] C. Yannouleas, E. Vigezzi, R.A. Broglia, Phys. Rev. B 47 (1993) 9849.
[6] A. Kornath, A. Kaufmann, A. Zoermer, R. Ludwig, J. Chem. Phys. 118 (2003) 6957.
[7] C. Bréchignac, P. Cahuzac, F. Carlier, J. Leygnier, Chem. Phys. Lett. 164 (1989) 433.
[8] C. Bréchignac, P. Cahuzac, J. Leygnier, A. Sarfati, Phys. Rev. Lett. 70 (1993) 2036.
[9] C. Bréchignac, H. Busch, P. Cahuzac, J. Leygnier, J. Chem. Phys. 101 (1994) 6992.
[10] P. Dugourd, D. Rayane, P. Labastie, B. Vezin, J. Chevaleyre, M. Broyer, Chem. Phys. Lett. 197 (1992) 433.
[11] E. Benichou, et al., Phys. Rev. A 59 (1999) R1.
[12] R. Antoine, D. Rayane, A.R. Allouche, M. Aubert-Frecon, E. Benichou, F.W. Dalby, P. Dugourd, M. Broyer, C. Guet, J. Chem. Phys. 110 (1999) 5568.
[13] B.K. Rao, P. Jena, Phys. Rev. B 32 (1985) 2058.
[14] B.K. Rao, P. Jena, M. Manninen, Phys. Rev. B 32 (1985) 477.
[15] F. Wang, N. Andriopoulos, N. Wright, E.I. Nagy-Felsobuki, J. Cluster Sci. 2 (1991) 203.
[16] I. Boustani, W. Pewestorf, P. Fantucci, V. Bonačić-Koutecký, J. Kouteck, Phys. Rev. B 35 (1987) 9437.
[17] O. Sugino, H. Kamimura, Phys. Rev. Lett. 65 (1990) 2696.
[18] S.E. Wheeler, H.F. Schaefer III, J. Chem. Phys. 122 (2005) 204328.
[19] G. Gardet, F. Rogemond, H. Chermette, J. Chem. Phys. 105 (1996) 9933.
[20] R. Fournier, J.B.Y. Cheng, A. Wong, J. Chem. Phys. 119 (2003) 9444.
[21] K.V. Jovan Jose, S.R. Gadre, J. Chem. Phys. 129 (2008) 164314.
[22] K.R.S. Chandrakumar, T.K. Ghanty, S.K. Ghosh, J. Phys. Chem. A 108 (2004) 6661.
[23] G. Mie, Ann. Phys. (Leipzig) 25 (1908) 377.
[24] J. Blanc, V. Bonačić-Koutecký, M. Broyer, J. Chevaleyre, P. Dugourd, J. Koutecký, C. Scheuch, J.P. Wolf, L. Wöste, J. Chem. Phys. 96 (1992) 1793.
[25] P. Dugourd, J. Blanc, V. Bonačić-Koutecký, M. Broyer, J. Chevaleyre, J. Koutecky, J. Pittner, J.P. Wolf, L. Wöste, Phys. Rev. Lett. 67 (1991) 2638.
[26] J.M. Pacheco, J.L. Martins, J. Chem. Phys. 106 (1997) 6039.
[27] S.A. Blundell, C. Guet, Z. Phys. D 33 (1995) 153.
[28] K. Yabana, G.F. Bertsch, Z. Phys. D 32 (1995) 329.

[29] J. Harris, Phys. Rev. B 31 (1985) 1770.
[30] B. Delley, J. Chem. Phys. 92 (1990) 508.
[31] J.P. Perdew, K. Burke, M. Ernzerhof, Phys. Rev. Lett. 77 (1996) 3865.
[32] J.E. Jaffe, Z. Lin, A.C. Hess, Phys. Rev. B 57 (1998) 11834.
[33] R. Berliner, S.A. Werner, Phys. Rev. B 34 (1986) 3586.
[34] A.D. Becke, J. Chem. Phys. 98 (1993) 5648.
[35] M.J. Frisch, et al., Gaussian, 03, Gaussian, Inc., Pittsburgh, Pennsylvania, 2003.
[36] G. Onida, L. Reining, A. Rubio, Rev. Mod. Phys. 74 (2002) 601.
[37] T.L. Beck, Rev. Mod. Phys. 72 (2000) 1041.
[38] K.P. Huber and G. Herzberg, Molecular Spectra and Molecular Structure. IV. Constants of Diatomic Molecules, (1979).
[39] M. Yang, K.A. Jackson, C. Koehler, T. Frauenheim, J. Jellinek, J. Chem. Phys. 124 (2006) 024308.
[40] J. Li, X. Li, H.-J. Zhai, L.-S. Wang, Science 299 (2003) 864.
[41] J. Wang, G. Wang, J. Zhao, Chem. Phys. Lett. 380 (2003) 716.
[42] C. Kittle, I. t. S. S. Physics, t. Ed, and J. W. (New York, 1986).
[43] W. Ekardt, Phys. Rev. B 29 (1984) 1558.